COMADEM 2014
16 – 18 September 2014 | Brisbane Convention and Exhibition Centre, Australia
27th International Congress of Condition Monitoring and Diagnostic Engineering

A Novel Method for the Fault Diagnosis of a Planetary Gearbox based on Residual Sidebands from Modulation Signal Bispectrum Analysis

Fengshou Gu[a,b,*] Gaballa M Abdalla[a], Riliang Zhang[b], Haijun Xu[c,a], and Andrew D. Ball[a]

[a]*Centre for Efficiency and Performance Engineering, University of Huddersfield, Huddersfield, HD1 3DH,UK*
[b]*School of Mechanical Engineering, Taiyuan University of Technology, Shanxi, China, 030024.*
[c]*School of Mechatronics and Automation, National University of Defense Technology, Hunan, China, 410073.*

ABSTRACT

This paper presents a novel method for the fault diagnosis of planetary gearboxes based on an accurate estimation of residual sidebands using a modulation signal bispectrum (MSB). The residual sideband resulting from the out-phase superposition of vibration waves from asymmetrical multiple meshing sources are much less influenced by gear errors than that of the in-phase sidebands. Therefore, with the accurate estimation by MSB they can produce accurate and consistent diagnosis, which are evaluated by both simulating and experimental studies. However, the commonly used in-phase sidebands have high amplitudes but include gear error effects, consequently leading to poor diagnostic results.

Keywords: Planetary gearbox, Residual sidebands, Condition Monitoring, Modulation signal bispectrum

* Corresponding author. Tel.: +44(0) 1484 473548, e-mail:f.gu@hud.ac.uk

1. Introduction

Planetary or epicyclic gearboxes are widely used in the power transmission of helicopters, automobiles, aircraft engines, heavy machinery and marine vehicles. Because planetary gearbox associated applications are so critical, condition monitoring of planetary gearboxes has received significant attention by many researchers. As shown in the general review paper by Lei et at [1-3], considerable works have been carried out on the investigation of vibration characteristics for monitoring various faults including gear pitting, crack and wear. In addition, many different signal processing methods in the time domain, frequency domain, time-frequency domain and advanced intelligent methods have been applied to analyze the complicated vibration signal for defining accurate and reliable diagnostic features [4-7]. However, it has been found that most of these works have developed the diagnostic parameters based on apparent vibration components which have large amplitudes in a spectrum and relate to fault dynamics. Especially, studies in [5] have shown that only the in-phase sideband components are useful for diagnosing different types of planetary gearbox faults.

Rather than using the apparent component for diagnosis, this paper focuses on the small sidebands which are usually not so noticeable in the spectrum. However, it will show that they contain reliable diagnostic information which is not influenced by inherent manufacturing errors. Firstly the paper demonstrates the existence and characteristics of these small sidebands by simulation studies. Then MSB is used to extract these sidebands accurately which are easily contaminated by random noise due to their small amplitudes. Finally an experimental investigation is carried out to show the effectiveness and outstanding performance of this approach in diagnosing different types of gear faults by comparing the results with that obtained from the in-phase sidebands.

2. Planetary Gearbox Vibration based Diagnosis

2.1. Characteristic Frequencies for Fault Diagnosis

As shown in Fig. 1, a common planetary gearbox, generally consists of three planet gears all of the same size, meshed with one sun gear and ring gear. The carrier is floating and affixed to the output shaft by means of splines which allow it to move axially as required for uniform load sharing between the three planetary gears. In this paper an industrial planetary gearbox detailed in Table 1 is focused for fault diagnosis study.

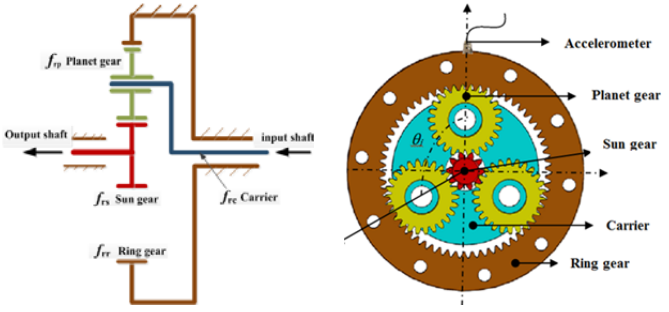

Figure 1. Schematic of a planetary gearbox

As shown by many previous studies, detection and diagnosis can be carried out by examining the change of fault characteristic frequencies around mesh frequency f_m and its harmonics. Considering that there are K number of planetary gears moving with carrier, characteristic frequencies around meshing frequency can be calculated [1] for three typical fault cases, which includes faults on the sun gear

$$f_{sf} = \frac{f_m}{z_s} = K(f_{rs} - f_{rc}) \quad (1)$$

faults on the planet gear

$$f_{pf} = 2\frac{f_m}{z_p} = 2(f_{rp} + f_{rc}) \quad (2)$$

and faults on the ring gear

$$f_{rf} = \frac{f_m}{z_r} = Kf_{rc} \quad (3)$$

Table 1. Planetary gearbox specification

No	Gear	Teeth	Frequency
1.	Ring	$z_r = 62$	$f_{rr} = 0$
2.	3x Planets	$z_p = 26$	f_{rp}
3.	Sun	$z_s = 10$	f_{rs}
4.	Input Shaft		f_{rc}
5.	Output Shaft		f_{rs}
6.	Transmission Ratio	7.2	
7.	Maximum Torque	670 *N·m*	
8.	Maximum input speed	2800 *rpm*	
9.	Maximum output speed	388 *rpm*	

However, as shown in [4-6] only some of these expected sidebands will be apparent in the vibration spectrum when a planetary gearbox has faulty because of the constructive effect of the vibration wave superposition between the three gear sets, whereas other sidebands are hard to be seen because of the destructive effect of the superposition and hence have been neglected by previous studies.

2.2. Characteristics of Residual Sidebands

According to the signal model developed in [5-7], a spectrum for a tooth defect on the sun gear is simulated based on a typical industrial planetary gearbox whose key specification is provided in Table 1. Fig. 2 shows the spectrum in the frequency range up to the third harmonics of mesh frequency. It shows that spectrum lines with high amplitudes at $1f_m - 7f_{sf}$, $1f_m - 6f_{sf} + 1f_{rc}$, $1f_m - 5f_{sf} - 1f_{rc}$ etc. and at $3f_m \pm 3f_{sf}$ and $3f_m \pm 6f_{sf}$ $3f_m \pm 6f_{sf}$ become larger due to the constructive effect of the in-phase superposition of the three vibration waves measured at the fixed ring gear casing. This is agreed with that predicted in [5] for indicating the fault of the sun gear. However, there are still many other observable spectral components which are not mentioned in [5]. Particularly, the components which locate symmetrically around the 1st and 2nd mesh frequencies at $1f_m \pm 3f_{sf}$, $1f_m \pm 6f_{sf}$, $2f_m \pm 3f_{sf}$ and $2f_m \pm 6f_{sf}$, illustrated by the arrows, are clearly visible. These components are well-known features which are used widely for the fault diagnosis of fixed shaft gearboxes. In order to examine the usefulness of these sidebands in diagnosing faults in planetary gearbox, they are named as residual sidebands in this study because they result from the in-complete superimposition of out-phase waves in the planetary gearbox. In contrast, the high amplitude sidebands such as those around the third mesh frequency at $3f_m \pm 3f_{sf}$ and $3f_m \pm 6f_{sf}$ are denoted as in-phase sidebands.

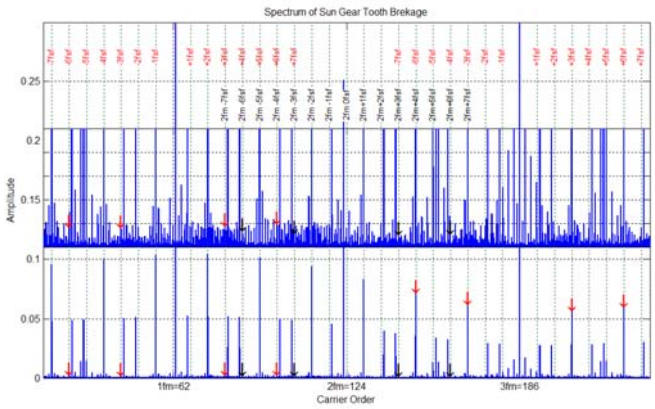

Figure 2 Spectrum for sun gear fault without error

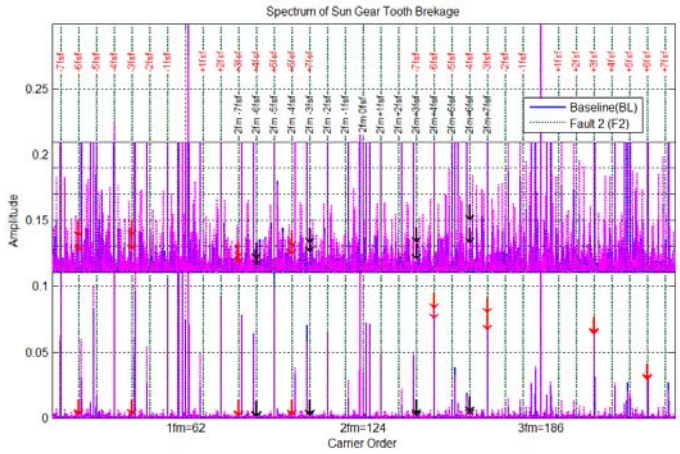

Figure 3 Spectrum for the case of sun gear fault with errors

Actually it is easy to understand the existence of the residual sideband. The development of the existing theory such as [5] for predicting fault components based on an assumption that the system is symmetrical perfectively. Thus it will give the zero amplitude for the residual sidebands. However, for considering a local fault on any of the gears and manufacturing errors, the symmetrical assumption does not hold true anymore. Consequently, the superimposition will result in non-zero components of the residual sidebands and at many other frequencies as shown in the magnified spectrum in Fig. 2. In practice, the system can never be symmetrical because of inevitable errors. It means that both the residual sidebands and the in-phase sidebands in measured signals will be influenced by the errors.

To examine the usefulness of these residual sidebands for fault diagnosis, a simulation was carried out for three cases, denoted as baseline (BL), Fault 1 (F1) and Fault 2 (F2), which are three successive steps of increasing the amplitude of tooth breakages. In addition, it also takes into account the effect of accumulative pitch errors of different gears. Fig.3 shows a comparison between two different cases. The in-phase components clearly show differences between the two cases. Obviously, the differences of the in-phase sidebands around $3f_m$, which are illustrated by the distance between the two arrows at the same spectral lines, can be used to differentiate the two cases. In the meantime, the residual sidebands, illustrated by the arrows in the magnified spectrum, also show sufficient differences so as to make a difference between the two cases. This shows that both types of sidebands can be good indicators for differentiating the faults.

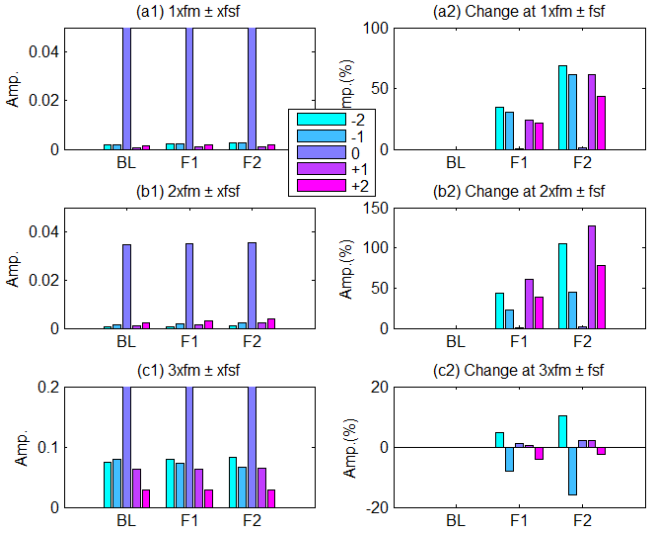

Figure 4 the comparison of sideband changes due to fault between different sidebands

To show the performance of using the residual sidebands for diagnosing the faults, the amplitudes at these sidebands are extracted from the spectrum and compared with that of the in-phase sidebands at the third harmonics. Fig. 4 presents these amplitudes against the fault cases and their relative changes with respect to their baselines. It shows that the residual sidebands around the first and the second mesh frequencies increase monotonically with the fault severities whereas the in-phase sidebands at the third mesh frequency exhibit a non-uniform change. Moreover the relative changes of the residual sideband are about five times higher than that of the in-phase sidebands. This means that the residual sidebands can produce a much better result in detecting and diagnosing the fault than that of the in-phase sidebands. This is mainly because the in-phase superimposition accumulates the effect of manufacturing errors simultaneously while it accumulates the effect of faults over three gear sets. For the small sideband amplitudes due to fault, the in-phase sideband will show a relative small change, either an increase or decrease depending on the agreement of phases between the sidebands due to errors and that due to fault. On the other hand the effect of errors is minimized at the residual sideband, any small changes due to faults will show significant corresponding changes. Therefore, the residual sidebands can potentially produce a consistent result with the fault severity and hence a more correct diagnosis.

2.3. Modulation Signal Bispectrum

However, as shown in the spectrum the residual sidebands have very low amplitudes and can be easily influenced by random noise. To extract them this study uses a modulation signal bispectrum spectrum based sideband estimator (MSB-SE), which has been developed recently by the authors [8] for characterizing the effects of modulation signals. MSB-SE is defined for a vibration signal $x(t)$ with corresponding Fourier Transform (FT) $X(f)$ as

$$B_{MS}^{SE}(f_s, f_c) = E[X(f_c + f_s)X(f_c - f_s) \\ X^*(f_c)X^*(f_c)/|X(f_c)|^2] \quad (4)$$

where the product between the upper sideband $X(f_c + f_s)$, the lower sideband $X(f_c - f_s)$ and the normalized carrier component $X^*(f_c)X^*(f_c)/|X(f_c)|^2$ allows the sideband effect to be combined and quantified without the effect of the carrier amplitude. Moreover, because of the average operation, denoted by the expectation operator $E[]$, the sideband products with a constant phase are enhanced, while the noise and interfering

components with random phases are suppressed. This MSB based approach has been shown to produce outstanding performance in characterizing the small modulating components in electrical current signals for diagnosing different electrical and mechanical faults [9-13].

3. Experimental Setups

3.1. Test Rig

The planetary gearbox was tested on a test rig shown in Fig. 5. It consists of a three phase induction motor of 11kW at 1465rpm, flanged in a cantilever type arrangement to a two stage helical gearbox, the planetary gearbox, two of flexible tyre coupling, and a DC generator for applying load to the gearbox. The helical gearbox is used as a speed reducer with a transmission ratio of 3.6 whereas the planetary gearbox is as an increaser with transmission ratio 7.2 so that the system can be loaded effectively by the DC motor.

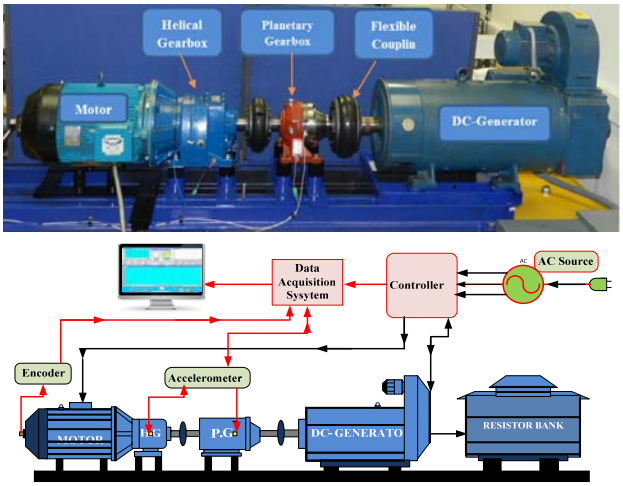

Figure 5. Planetary gearbox test rig and the schematic of test system

The Fig. 5 shows the schematic diagram of the planetary gearboxes test system and the position of the accelerometers. The shaft encoder at the end of the induction motor shaft produces 100 pulses per revolution for measuring the speed of the system which is based for identifying characteristic frequencies of gearbox vibration. Furthermore, a digital variable speed controller is attached to the test rig between the AC power line source and the motor to control the speed of the testing motor. The controller can be programmed to any specific shaft rotation speed between 0 to 1465rpm and load between 0% and 90% of full load.

3.2. Data Acquisition

To examine the influence of the operating condition on fault diagnosis performance the tests were carried out when the speed of the AC motor was at 40% of the full speed. Considering the transmission ratio, the planetary gearbox will operates at 80% of its full speed correspondingly. At each speed the system is loaded under five successive loads (0%, 25%, 50%, 75% and 90% of the full load). These operating conditions will allow an exploration of different load influences on vibration contents for developing a reliable diagnostic method.

The vibration is measured by an accelerometer type PCB 338C04 on the housing of the planetary gearbox with the sensitivity of 100 mv/g, and frequency response ranges from 1Hz to 10 kHz. All the data are logged simultaneously by a multiple channel, high speed data acquisition system operating at 100 kHz rate and 16bit resolution.

3.3. Gear Faults

Two tests were carried out to examine the tooth faults on the sun and planet gears respectively. The first is for testing different sizes of defects on one tooth of the sun gear and the second is for testing different sizes of defects on the planet gear tooth. A baseline measurement was firstly carried out when the gears were healthy i.e. without any defects induced. Then the second measurement was completed when a defect on the sun gear was created manually by damaging single surface of the tooth by 30% of the full teeth width. The third measurement was for the case of increasing the defects up to 60%. For the convenience of discussion these three cases are denoted as BL, F1 and F2 respectively. Fig. 4(a) shows the two defects respectively.

In the same way, one of the planetary gears was tested under its baseline and two increments of tooth defects. Fig. 4(b) shows the two defects respectively, which was simulated on one side of the gear..

In addition, both the tests for the sun gear fault and planet gear fault were conducted on the same gearbox casing but with two different sets of gears for comparison.

(a) Sun gear defect (b) Planet gear defect

Figure 6. Different defects simulated on the sun and planet gears

4. Diagnostic Results and Discussion

4.1. Spectrum of Vibration Signals

Fig. 7 shows typical spectra from the sun gear fault tests. It can be seen that three distinctive peaks close to the first three mesh frequencies appear at $f_m + f_{rc}$, $2f_m - f_{rc}$ and $3f_m$, which are agreed with that from prediction. However, there are also many distinctive peaks between two mesh frequencies. For example, the components at $2f_m - 6f_{sf} - 1f_{rc}$, $2f_m + 7f_{sf}$ etc. are supposed not to appear for a healthy planetary gearbox. Therefore, based on the simulation studies in Section 2, these peaks indicate that the gearbox has significant manufacturing errors. It means that the diagnosis based on the in-phase sideband may not be accurate, which can be demonstrated by examining the changes at $3f_m \pm 3f_{sf}$ and $3f_m \pm 6f_{sf}$ between the three cases.

To examine the changes of the residual sidebands, their amplitudes including that at the in-phase components are extracted and presented in Fig. 8. Because of the attenuation of vibration transfer function, the spectrum show very low amplitude below $1f_m$, which is also the general feature of acceleration responses. So the residual sidebands around $1f_m$ are not explored because of their low signal to noise ratios. Based on the changes of these sidebands, it can be found that the amplitudes of the second order residual sidebands around $2f_m$ and those at $2f_m$ may be good indicators for the fault severity as their amplitude show an increasing change which agrees with the fault severities at high load conditions.

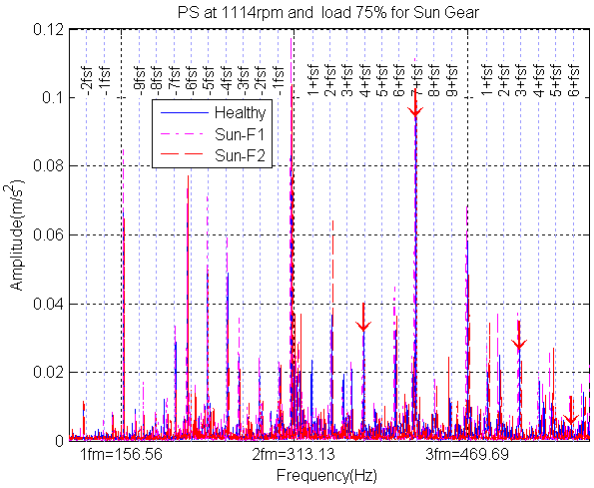

Figure 7. Spectrum for different fault cases of the sun gear

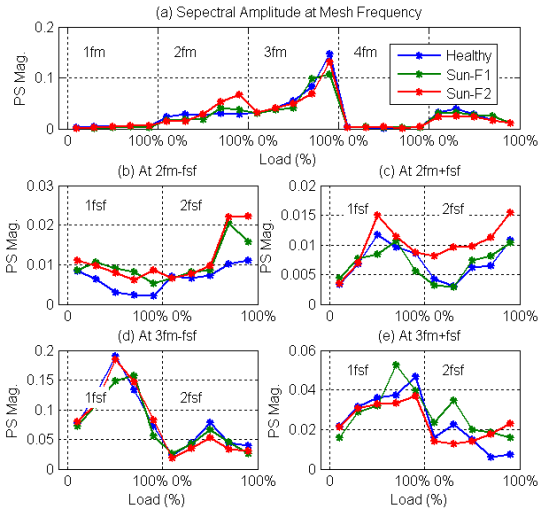

Figure 8. Spectral amplitudes of different sidebands and mesh frequencies

In contrast, the amplitudes of other sidebands and meshing components exhibit very high fluctuations between fault cases and loads. So they cannot be used for obtaining a consistent diagnostic result. Especially, the in-phase sidebands around $3f_m$ show high amplitudes but with less relative changes between fault cases, showing that they are not good indicators for the faults.

In general, the residual sidebands show better diagnostic results, compared with that of the in-phase sideband. However, as shown in Fig. 8 (b) and (c) these residual sidebands still cannot differentiate F1 from the baseline appropriately.

4.2. MSB of Vibration Signals

To improve the diagnostic results, MSB analysis is applied to corresponding signals. Fig. 9 shows typical MSB results for the three sun gear tests under a load of 75%. To show a clear change of the residual sidebands around mesh frequency $2f_m = 313Hz$ MSB and its corresponding coherence results are presented in the bifrequency domain in the region of $f_c \leq 2f_m \pm 1 = 313 \pm 1Hz$ and $f_s < 100Hz$ to include the sidebands up to $6f_{sf}$. It can be seen in Fig.9 that the magnitude of many MSB peaks increase with the fault severities. In particular, peaks at bifrequencies $(2f_m, 5f_{sf})$ and $(2f_m, 5f_{rc})$ show very distinctive amplitudes which vary consistently with the faults. However, these two peaks are also the in-phase sidebands and influenced more by errors, which will be shown in further content. Therefore, they are not considered in this study. Instead it is the residual sidebands at $(2f_m, 3f_{sf})$ and $(2f_m, 6f_{sf})$ that are interesting in this study. As illustrated by the size of the arrows, although these sidebands have small amplitude, they show consistent changes with the sizes of faults. Furthermore, these small amplitudes are fully supported by high amplitudes of their corresponding coherence.

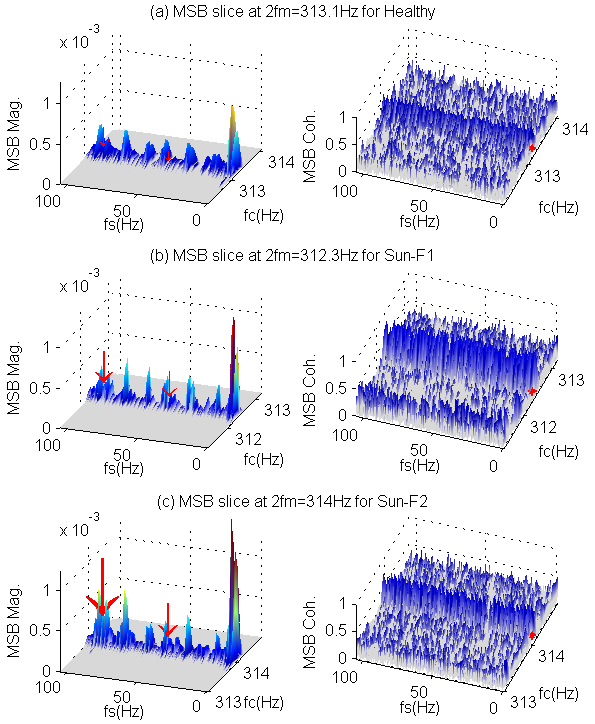

Figure 9. MSB results for different cases of the sun gear tests

Moreover, these changes can shows a clear difference between the F1 and baseline which could not be separated by the spectral amplitude shown in Fig. 8. This demonstrates that MSB analysis allows more accurate sideband estimate because of its effect of noise suppression.

4.3. Diagnosis of Sun Gear Fault

To explore the performance of the residual sidebands obtained by MSB analysis, the peak values at the corresponding characteristic frequencies for planetary gearbox diagnosis are extracted from MSB results and presented in Fig. 10. From the results of residual sidebands obtained from the MSB slice at $2f_m$, it can be seen that the amplitudes at f_{sf} show a good increasing trend with loads, which agrees with the load characteristics. Moreover, these amplitudes show clear incremental differences between three tested cases. Therefore, they can be used for obtaining fault diagnosis reliably.

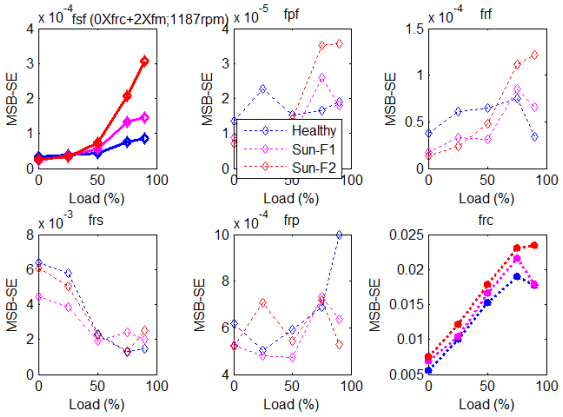

(a) Results from the sidebands around $2f_m$

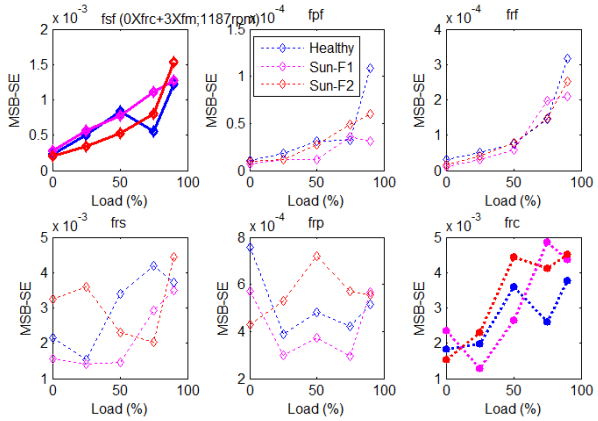

(b) Results from the in-phase-sidebands around $3f_m$

Figure 10 MSB diagnosis results of the sun gear faults

In addition, the MSB results at f_{rc} also show similar results with that at f_{sf} . It may show that the fault on the sun gear may also cause changes on the dynamics of the carrier. However, because the amplitude for the case of F1 has a clear drop under high load, it indicates that these sidebands are also influenced by the errors as that of the in-phase sidebands.

For comparison, the results from in-phase sidebands around $3f_m$ are also presented in Fig. 10(b). As shown by the amplitudes at f_{sf} , these in-phase sidebands cannot indicate the incremental changes caused by the faults consistently, which agrees with that from simulation.

4.4. Diagnosis of Planet Gear Fault

From the above discussion and diagnostic results, it can be drawn that the residual sideband based method is reliable for planetary gearbox diagnosis. To evaluate its performance further, the method is applied to the datasets from the planet gear test. Fig. 11 shows the spectrum of the vibration for the three cases of planet gear fault. Compared with the spectrum in Fig. 7, it exhibits clear differences. Particularly the spectrum amplitudes at $2f_m - 6f_{sf} - 1f_{rc}$, $2f_m + 7f_{sf}$ are significantly lower. This shows that this set gear may have a lower error distribution. Even though, the results from conventional spectrum based method cannot give a correct diagnostic results to be consistent with the fault severities induced as explained in Section 3.3 .

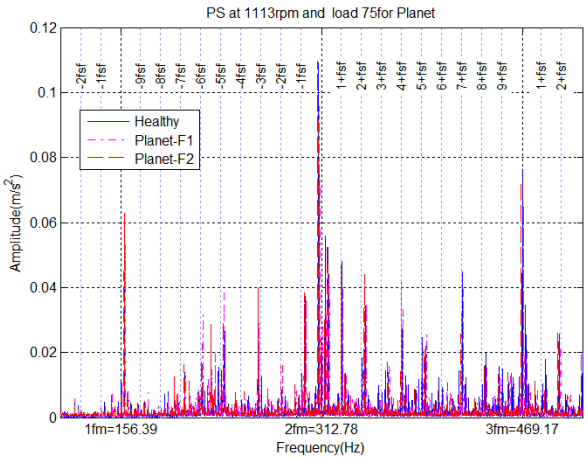

Figure 11. Spectrum for different fault cases of the planet gear

Fig. 12 presents the MSB based diagnostic results obtained from the residual sideband at $1f_m$, rather than $2f_m$ for the sun gear fault case. This is because that these sidebands exhibit more the features of residual sidebands, i.e. lower amplitude and less sensitive to the gear error. In addition, they also have less interfering components compared with that around the $2f_m$. As shown in the figure the MSB peaks at planet gear fault frequency f_{pf} show results which increases with fault severities and loads, resulting in correct diagnosis. In the meantime, the sidebands at f_{rp} also exhibit an increasing change, which may be a secondary feature for the fault on the planetary gear.

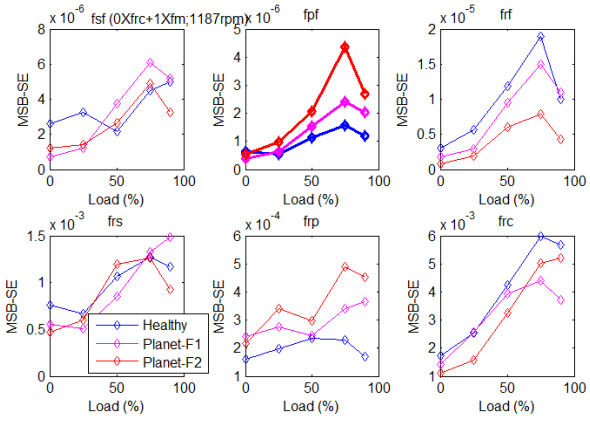

(a) Results from the residual sidebands around $1f_m$

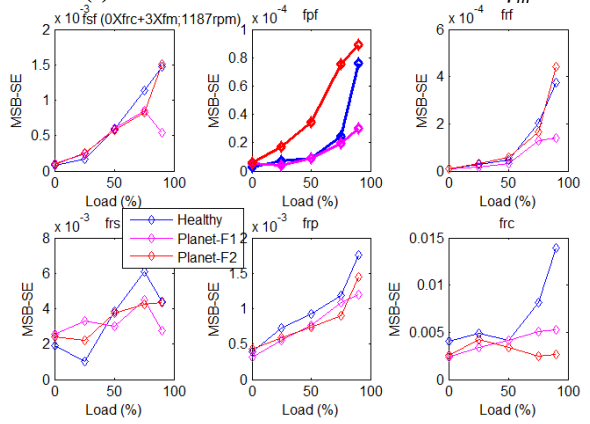

(b) Results from the in-phase sidebands around $3f_m$

Figure 12. MSB diagnosis results for different planet gear faults

On the other hand, the in-phase sidebands around $3f_m$ are able to separate the severer fault because the gear error is less than that of the sun gear fault case. However, they cannot separate the smaller fault. This proves further that the residual sideband has more reliable diagnostic information than that of the in-phase-sidebands.

5. Conclusion

The residual sidebands of the planetary gearbox result from the imperfect superposition of the vibrations from multiple meshing sources which are asymmetrical in nature. Although the amplitude of the residual sidebands are relatively small, compared with that of in-phase one, they are much less influenced by investible gear errors. Using the modulation signal bispectrum, these small sidebands can be estimated with a good degree of accuracy and hence produce more accurate and consistent diagnostic results. Both simulating and experimental results have shown that this sidebands based method provides correct diagnostic results for different sizes of faults on either the sun gear or the planet gear. On the other hand, the in-phase sidebands only give correct diagnostic results when the fault is larger than the effect of gear errors.

Acknowledgments

The research is supported partly by the Natural Science Foundation of China under the Grant No. 51375326.

References

1. Lei, Y.; Lin, J.; Zuo, M.; He, Z. Condition monitoring and fault diagnosis of planetary gearboxes: A review. Measurement, 2014; Vol. 48, pp 292-305.
2. Samuel, P. D.; Pines, D. J. A review of vibration-based techniques for helicopter transmission diagnostics. Journal of Sound and Vibration, 2005; Vol. 282, pp 475–508.
3. Yuksel, C.; Kahramanb, A. Dynamic tooth loads of planetary gear sets having tooth profile wear. Mechanism and Machine Theory, 2004; Vol. 39, pp 697-715.
4. McFadden, P. D. A technique for calculating the time domain averages of the vibration of the individual planet gears and the sun gear in an epicyclic gearbox. Journal of Sound and Vibration, 1991; Vol. 144, pp 163-172.
5. Liu, H.; Dhupia, J. S.; Sheng, Sh. An explanation of frequency features enabling detection of faults in equally spaced planetary gearbox. Mechanism and Machine Theory, 2014; Vol. 73 pp 169-183.
6. McFadden, P. D.;.Smith, J. D. An explanation for the asymmetry of the modulation sidebands about the tooth meshing frequency in epicyclic gear vibration. Institution of Mechanical Engineers, 1985; Vol. 199, pp 65-70.
7. Inalpolat, M.; Kahraman, A. A theoretical and experimental investigation of modulation sidebands of planetary gear sets. Journal of Sound and Vibration, 2009; Vol. 323, pp 677-696.
8. Gu, F.; Wang, T.; Alwodai, A.; Tian, X.; Shao, Y.; Ball, A. D. A new Method of Accurate Broken Rotor Bar Diagnosis based on Modulation Signal Bispectrum Analysis of Motor Current Signals, Accepted by MSSP march 2014.
9. Cheng, Z.; Hu, N.; Gu, F.; Qin, G. Pitting Damage Levels Estimation for Planetary Gear Sets Based On Model Simulation and Grey Relational Analysis. Transactions of the Canadian Society for Mechanical Engineering, 2011; Vol. 35, pp 403-417.
10. Haram, M., Wang, T., Gu, F. and Ball, A.D. (2011) 'An Investigation of the Electrical Response of A Variable Speed Motor Drive for Mechanical Fault Diagnosis. Proceedings of the 24th International Congress on Condition Monitoring and Diagnostic Engineering Management (COMADEM 2011). : COMADEM. pp. 867-874.
11. Alwodai, A.; Gu, F.; Ball, A. D. A Comparison of Different Techniques for Induction Motor Rotor Fault Diagnosis. Journal of Physics: Conference Series, 2012; Vol. 364, pp 1742-6596.
12. Chen, Z.; Wang, T.; Gu, F.; Mansaf, H.; Andrew, B. D. Gear Transmission Fault Diagnosis Based on the Bispectrum Analysis of Induction Motor Current Signatures. Journal of Mechanical Engineering, 2012; Vol. 48, pp 84-90.
13. Alwodai, A.; Xia, X.; Shao, Y.; Gu, F.; Adrew, B. D. Modulation Signal Bispectrum Analysis of Motor Current Signals for Stator Fault Diagnosis. 18th International Conference on Automation and Computing (ICAC), 2010 . Loughborough, UK, IEEE. pp 1-6.